

Volume 52, Issue 11, November 2010 ISSN 0010-938X



CORROSION SCIENCE

The Journal on Environmental Degradation of Materials and its Control
Editor-in-Chief: G. T. BURSTEIN, University of Cambridge, U.K.
An Official Journal of the Institute of Corrosion

CONTENTS

A. FIROOZI and K. SHIRVANI	3579	The structure and high temperature corrosion performance of medium-thickness aluminide coatings on nickel-based superalloy GTD-111
D. K. YADAV, B. MAITI and M. A. QURASHI	3586	Electrochemical and quantum chemical studies of 3,4-dihydropyrimidin-2(1H)-ones as corrosion inhibitors for mild steel in hydrochloric acid solution
T.-M. WEN, K.-H. HOU, C.-Y. BAL, M.-D. GEE, P.-H. CHEN and S.-J. LEE	3599	Corrosion behaviour and characteristics of reforming chromized coatings on SS 420 steel in the simulated environment of proton exchange membrane fuel cells
T. NISHIMURA	3609	Electrochemical behaviour and structure of rust formed on Si- and Al-bearing steel after atmospheric exposure
M. REFFAÏS, C. BORZIOI, C. REHÉRIÉ, A. BILLARD and J. CREUS	3615	Corrosion behaviour of magnetron-sputtered Al _{1-x} Mn _x coatings in neutral saline solution
H. J. MARTIN, M. F. HÖRSTEMEYER and P. T. WANG	3624	Comparison of corrosion pitting under immersion and salt-spray environments on an as-cast Al34 magnesium alloy
H. CHEN, J. LIU and W. HUANG	3639	The protective surface film formed on molten ZK60 magnesium alloy in 1,1,1,2-tetrafluoroethane/air atmospheres
Z. FENG, X. CHENG, C. DONG, L. XU and X. LI	3646	Passivity of 316L stainless steel in borate buffer solution studied by Mott-Schottky analysis, atomic absorption spectrometry and X-ray photoelectron spectroscopy
W. KUANG, E.-H. HAN, X. WU and J. RAO	3654	Microstructural characteristics of the oxide scale formed on 304 stainless steel in oxygenated high temperature water
R. M. PIDAPARTI, B. S. AGRAZADEH, A. WHITEFIELD, A. S. RAO and G. P. MENCHER	3661	Classification of corrosion defects in NiAl bronze through image analysis
W. QAFRAOUI and H. TAKENOUTI	3667	Corrosion protection of 2024-T3 aluminium alloy by electro-polymerized 3-amino 1,2,4-triazole in sulphate solution containing chloride
C. LI, Y. MA, Y. LI and F. WANG	3677	EIS monitoring study of atmospheric corrosion under variable relative humidity
M. LIU, P. SCHMITZ, P. J. UGGOWITZER, G. SONG and A. ATRENS	3687	The influence of yttrium (Y) on the corrosion of Mg-Y binary alloys

Contents continued on outside back cover
<http://www.elsevier.com/locate/corsci>

This article appeared in a journal published by Elsevier. The attached copy is furnished to the author for internal non-commercial research and education use, including for instruction at the authors institution and sharing with colleagues.

Other uses, including reproduction and distribution, or selling or licensing copies, or posting to personal, institutional or third party websites are prohibited.

In most cases authors are permitted to post their version of the article (e.g. in Word or Tex form) to their personal website or institutional repository. Authors requiring further information regarding Elsevier's archiving and manuscript policies are encouraged to visit:

<http://www.elsevier.com/copyright>



Contents lists available at ScienceDirect

Corrosion Science

journal homepage: www.elsevier.com/locate/corsci

Short Communication

Effect of surface nanocrystallization on the corrosion behaviour of AISI 409 stainless steel

T. Balusamy, Satendra Kumar, T.S.N. Sankara Narayanan*

National Metallurgical Laboratory, Madras Centre, CSIR Madras Complex, Taramani, Chennai 600 113, India

ARTICLE INFO

Article history:

Received 28 January 2010

Accepted 5 July 2010

Available online 31 July 2010

Keywords:

A. Steel

B. EIS

B. Polarization

B. XRD

C. Passivity

ABSTRACT

The influence of surface mechanical attrition treatment (SMAT) on the corrosion behaviour of AISI 409 grade stainless steel in 0.6 M NaCl was studied. SMAT using 2 mm \varnothing 316L stainless steel (SS) balls for 15, 30 and 45 min and 5 mm \varnothing balls for 15 min offers a better corrosion protective ability. In contrast, treatment using 5 mm \varnothing balls for 30 and 45 min and by using 8 mm \varnothing balls for 15, 30 and 45 min, induces microstrain and defect density that results in a decrease in corrosion resistance.

© 2010 Elsevier Ltd. All rights reserved.

1. Introduction

Nanocrystalline (NC) materials have received considerable attention, as they are fundamentally different from their conventional polycrystalline counter parts in terms of properties such as, high hardness and strength, enhanced electrical resistivity, higher thermal expansion coefficient, higher heat capacity, improved tribological properties, better fatigue properties, super plasticity at low temperature, etc. [1–3]. Numerous techniques such as ball milling, chemical vapour deposition, physical vapour deposition, electrodeposition, crystallization of amorphous solids, etc., were developed for preparing bulk NC materials [1,4]. However, it is important to note that most of the material related failures such as, fatigue fracture, fretting fatigue, wear, corrosion, etc., occur on the surface and they are very sensitive to the structure and properties of those materials. Hence, optimization of the microstructure and properties by means of various surface modification techniques is necessary to enhance the global behaviour and lifetime of materials. Surface mechanical attrition treatment (SMAT) is a novel surface treatment method, which enables the formation of a nanostructured surface layer on metallic materials in order to improve the overall properties and performance [5,6]. In this method, nanocrystallization of the surface occurs by the grain refinement mechanism induced by plastic deformation.

The corrosion behaviour of nanocrystalline materials and coatings is an interesting area of research [7–10]. The plastic deformation induced by SMAT or other treatment methods such as cold

rolling, cold working, extrusion, shot peening, ultrasonic peening, equal channel angular extrusion (ECAE), equal channel angular pressing (ECAP), etc., has been shown to significantly influence the corrosion resistance of metallic materials [11–20]. It has been reported that plastic deformation has a detrimental effect on the corrosion resistance of stainless steels due to the formation of defective interfaces and defects in the grains resulted from the accumulation of internal stresses during the deformation process [21,22]. Similarly, plastic deformation has been shown to decrease the corrosion resistance of AZ31 magnesium alloy [19]. However, plastic deformation has been shown to have a beneficial effect on the corrosion resistance of high strength cast iron because the change in shape of graphite after deformation results in a surface with a small number of inclusions per unit area [23]. Hence, evaluation of the corrosion behaviour of metallic materials subjected to SMAT will be an interesting area of research.

Li et al. [11] have shown that surface nanocrystallization of low carbon steel by SMAT decreased their corrosion resistance in 0.05 M H₂SO₄ + 0.05 M Na₂SO₄. SMAT has been shown to introduce surface defects, prevents the formation of passive film and deteriorate the corrosion resistance of AISI 316 stainless steel in 0.1 M NaCl [12]. The formation of nanocrystalline boundaries by SMAT leads to a reduction in corrosion resistance whereas the formation of twin boundaries enables an improvement in corrosion resistance of AISI 316L stainless steel in 0.05 M H₂SO₄ + 0.25 M Na₂SO₄ [13]. Hence, it appears that the effect of surface nanocrystallization by SMAT on the corrosion performance is a function of the nature of the materials and environment. The corrosion behaviour of AISI 409 grade stainless steel (AISI 409 SS) subjected to SMAT has not been studied earlier. In this perspective, the present work aims

* Corresponding author. Tel.: +91 44 2254 2077; fax: +91 44 2254 1027.
E-mail address: tsnsn@rediffmail.com (T.S.N. Sankara Narayanan).

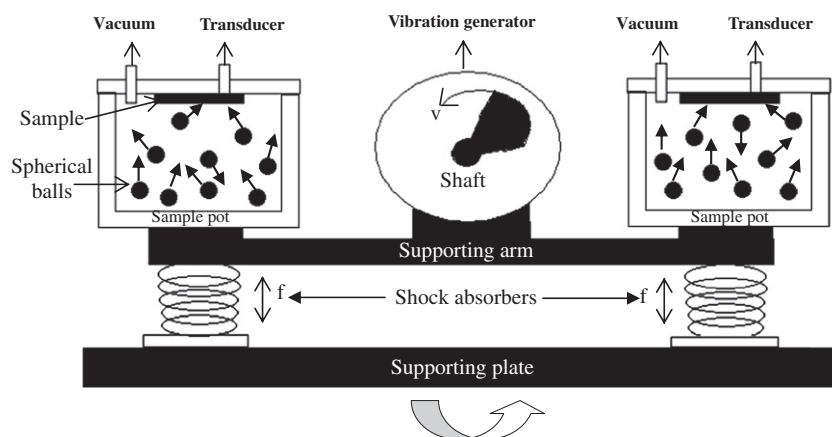


Fig. 1. Schematic of the surface mechanical attrition treatment (SMAT) set-up.

to evaluate the effect of SMAT on the corrosion behaviour of AISI 409 SS in 0.6 M NaCl.

2. Experimental details

AISI 409 SS discs (65 mm \varnothing and 2 mm thick), having a chemical composition of (in wt.%) C: 0.01; Si: 0.01; Mn: 0.029; P: 0.020; S: 0.008; Cr: 10.51; Mo: 0.02; Ni: 0.10; Al: 0.05; Cu: 0.11; Ti: 0.19; V: 0.02; Mg: 0.02; Zn: 0.01; Fe: balance; were used as substrate materials. The samples were degreased using acetone. SMAT of AISI 409 SS was performed using the surface nanocrystallization equipment (Model: SNC1, Chengdu SNC Advanced Technology Co., Ltd., Chengdu, China). The schematic of SMAT set-up is shown in Fig. 1. AISI 409 SS sample was fixed in the upper part of the sample pot whereas AISI 316L grade SS balls (2, 5 and 8 mm \varnothing) were kept at the bottom. The distance between the sample and the balls were about 25–30 mm. The sample pot was evacuated and kept under vacuum during the entire period of treatment. The sample pot was connected to a vibration generator. The frequency of vibration was kept constant at 50 Hz. When the balls resonate with the vibration frequency, they start to fly and impinge on the sample surface. Since the balls were confined within the sample pot, their impact on the sample surface would be random and multidirectional. The SMAT was performed for 15, 30 and 45 min. The methodology of SMAT was already described in detail by Lu and Lu [5,6]. The surface profile of untreated and SMATed AISI 409 SS discs was measured using a surface profilometer (Mitutoyo SJ 301). The surface topography of the treated samples was assessed by atomic force microscopy (AFM). The grain size and the mean microstrain induced during treatment were determined by X-ray diffraction (XRD) measurement (Model: D-8 Discover, Bruker AXS) using $\text{Cu-K}\alpha$ radiation.

The corrosion behaviour of untreated and treated samples in 0.6 M NaCl was evaluated by open circuit potential (OCP)–time measurement, potentiodynamic polarization, electrochemical impedance spectroscopy (EIS) and current–time transient (CTT) studies. Either untreated or SMATed samples form the working electrode while a saturated calomel electrode (SCE) and a graphite rod were used as the reference and auxiliary electrode, respectively. These three electrodes were placed within a flat cell (Friction and Wear Tech., Chennai) in such a way that only 1 cm² area of the working electrode was exposed to the electrolyte solution. Potentiodynamic polarization measurements were carried out in the potential range from $-500 \text{ mV}_{(\text{SCE})}$ in the cathodic direction to $+2000 \text{ mV}_{(\text{SCE})}$ in the anodic direction from open circuit potential (OCP) at a scan rate of 100 mV/min. The scan rate used for polarization study is an

important parameter and if not chosen properly it would incorrectly reflect the corrosion process. During the corrosion process, the electrode surface can be considered as a simple resistor (solution resistance) in series with a parallel combination of a resistor (polarization resistance) and capacitor (double layer capacitance). Hence, the scan rate should be slow enough so that the capacitors remain fully charged and the current/voltage relationship reflects only the interfacial corrosion process at every potential of the polarization scan. Otherwise, it would reflect charging of the surface capacitance in

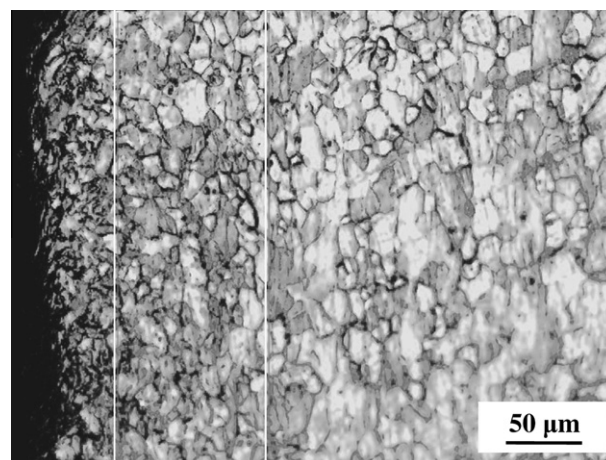


Fig. 2. Formation of a graded layer structure on AISI 409 SS after SMAT using 8 mm \varnothing balls for 45 min.

Table 1

Surface roughness of untreated AISI 409 SS and samples SMATed using 2, 5 and 8 mm \varnothing 316L SS balls for 15, 30 and 45 min.

Treatment condition of the AISI 409 SS	Surface roughness (μm)		
	R_a	R_z	R_q
Untreated	0.33	3.60	0.49
SMAT using 2 mm \varnothing 316L SS ball for 15 min	0.54	3.27	0.67
SMAT using 2 mm \varnothing 316L SS ball for 30 min	0.60	3.56	0.74
SMAT using 2 mm \varnothing 316L SS ball for 45 min	0.55	3.02	0.68
SMAT using 5 mm \varnothing 316L SS ball for 15 min	0.80	4.27	0.97
SMAT using 5 mm \varnothing 316L SS ball for 30 min	0.85	4.43	1.04
SMAT using 5 mm \varnothing 316L SS ball for 45 min	0.88	4.59	1.07
SMAT using 8 mm \varnothing 316L SS ball for 15 min	1.48	8.71	1.87
SMAT using 8 mm \varnothing 316L SS ball for 30 min	1.33	7.69	1.65
SMAT using 8 mm \varnothing 316L SS ball for 45 min	1.69	9.87	2.08

addition to the corrosion process. In such conditions, the measured current would be greater than the current actually generated by the corrosion reactions. The estimated maximum scan rates for several combinations of polarization resistances, solution resistances, and capacitances, which are often encountered in practice is compiled by Silverman [24]. Accordingly, for a combination of solution resistance, charge transfer/film resistance and capacitance of 10 Ohm cm^2 , $10^3\text{--}10^4 \text{ Ohm cm}^2$ and $100 \mu\text{F}$, the recommended scan rate lies between 0.51 and 5.1 mV/s. In the present study, a scan rate of 100 mV/min (i.e., 1.67 mV/s.) is used. Moreover, while choosing the scan rate for polarization study, one should maintain an appropriate balance between the slow scan rates and quickly get the required information. In addition, the scan rates should be kept similar to ensure consistent comparison between untreated and

treated samples in a given environment. A scan rate of 100 mV/min has been used in our earlier studies [25–29] as well as by other researchers [16,30]. The corrosion potential (E_{corr}) and corrosion current density (i_{corr}) were determined using Tafel extrapolation method. EIS studies of the untreated and treated samples were performed at their respective OCPs. The impedance spectra were obtained using an excitation voltage of 32 mV rms (root mean square) in the frequency range between 10 kHz and 0.01 Hz. The choice of this amplitude was made as it would yield better results than 4 mV [31]. The EIS parameters were determined from the Nyquist plot after fitting the data using BOUKAMP software. CTT were recorded at $-100 \text{ mV}_{(\text{SCE})}$ for 1800 s. The electrochemical studies were repeated at least three times to ensure reproducibility of the test results. The surface morphology of the SMATed samples (using 2, 5 and

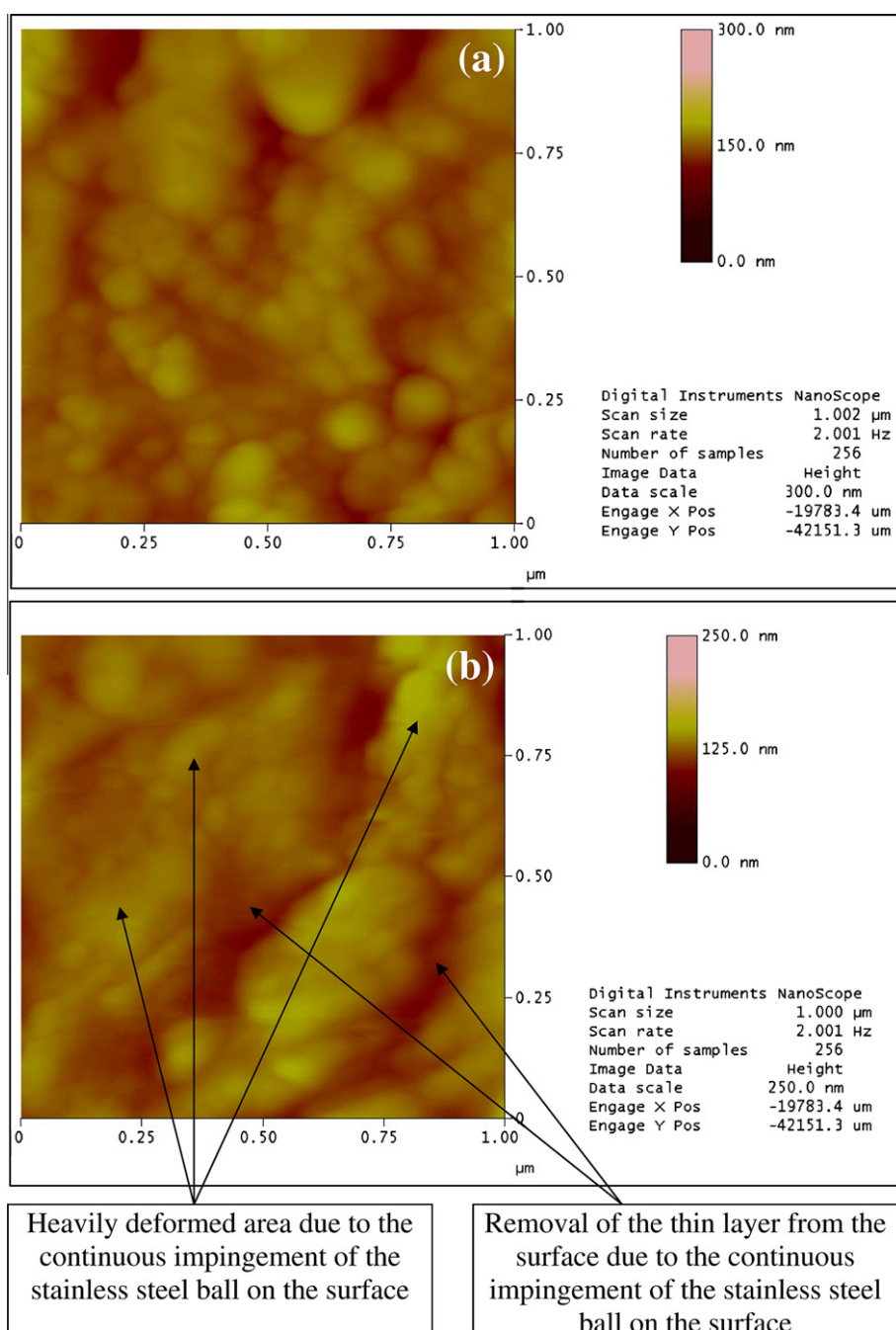


Fig. 3. Surface topography of AISI 409 SS sample after SMAT using 8 mm \varnothing balls for (a) 15 min; and (b) 45 min.

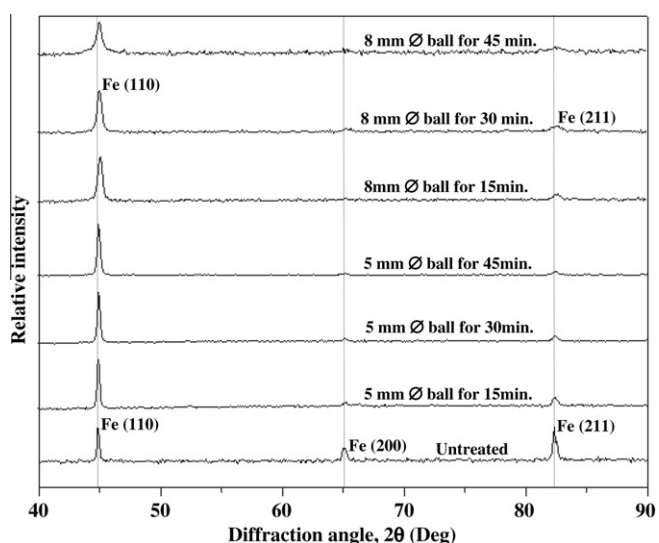


Fig. 4. XRD patterns of AISI 409 SS – untreated and after SMAT using 5 and 8 mm \varnothing balls for various duration of time.

8 mm balls for 15 min) after polarizing them from -250 to $+250$ mV_(SCE) from their respective OCPs in 0.6 M NaCl was assessed using scanning electron microscopy (SEM).

3. Results and discussion

3.1. Characteristics of AISI 409 SS subjected to SMAT

During SMAT, impingement of the 316L SS balls on the surface of the AISI 409 SS sample induces plastic deformation with a high strain rate during each impact. The thickness of the nanostructured surface layer is found to be a function of the size of the ball and treatment time. SMAT enables the formation of a graded layer structure with nano-sized grains at the surface and sub-micron/micron sized grains at the intermediate region whereas the grains at the bulk remain largely unaffected. The graded layer structure formed on AISI 409 SS subjected to SMAT using 8 mm balls for 45 min is shown in Fig. 2. The surface roughness of untreated

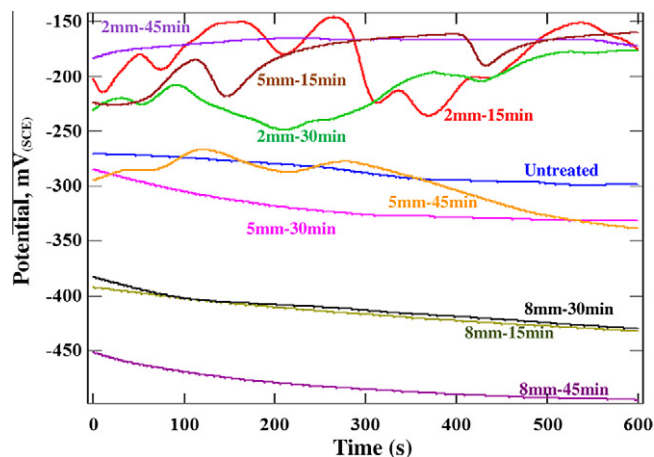


Fig. 6. OCP–time curves of AISI 409 SS in 0.6 M NaCl – untreated and after SMAT using 2, 5 and 8 mm \varnothing balls for various duration of time.

and treated samples is given in Table 1. SMAT increased the surface roughness and the extent of increase in roughness is a function of the size of the balls and treatment time. In general, increase in ball size and treatment time increases the roughness. The increase in roughness with treatment time is further confirmed by the surface topography assessed by AFM (Fig. 3). The XRD patterns of untreated and treated (5 and 8 mm balls for 15, 30 and 45 min) samples are shown in Fig. 4. Untreated sample exhibits peaks pertaining to Fe (110), Fe (200) and Fe (211) planes whereas a reduction in intensity of the Fe (200) and Fe (211) planes and broadening of the peaks pertaining to all the three planes are observed for treated samples. A small shift in the diffraction angle is observed for samples treated using 8 mm balls. The broadening of the peaks and shift in diffraction angle could be due to the increase in crystallite imperfections/defect density and increase in microstrain induced during SMAT. This observation is further supported by the heavy deformation observed by AFM (Fig. 3b). The average grain size and the mean microstrain measured as a function of treatment time (Fig. 5) reveal that an increase in treatment time from 15 to 30 min leads to a decrease in grain size and a slight increase in microstrain. Further increase in treatment time from 30

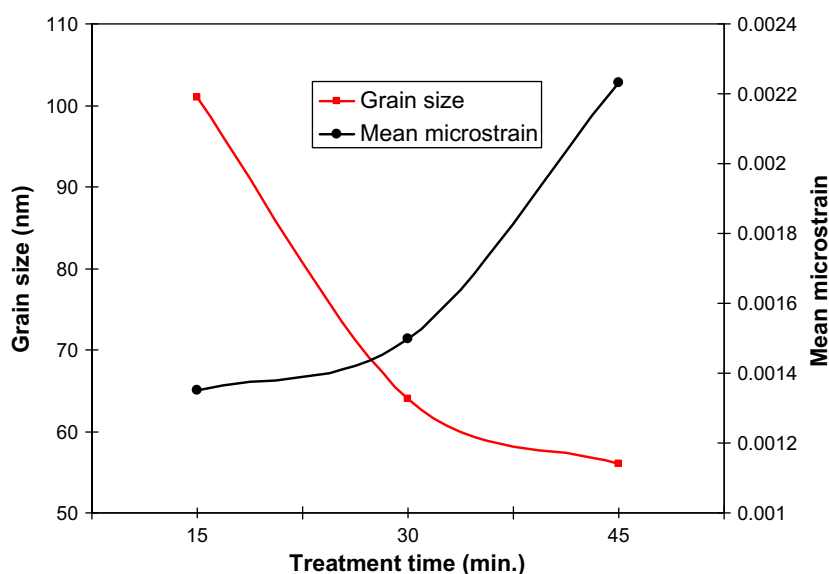


Fig. 5. Change in average grain size and the mean microstrain of AISI 409 SS after SMAT using 5 mm \varnothing balls as a function of treatment time.

to 45 min has resulted in a slight reduction in grain size but a significant increase in the mean microstrain.

3.2. Corrosion behaviour of AISI 409 SS subjected to SMAT

The change in open circuit potential (OCP) of untreated and treated samples measured as a function of time, is shown in Fig. 6. The potentiodynamic polarization curves of these samples are shown in Fig. 7. The corrosion potential (E_{corr}) and corrosion

current density (i_{corr}), are compiled in Table 2. Compared to the untreated one, samples SMATed using 2 mm balls at all treatment times studied and those treated using 5 mm balls for 15 min exhibit an anodic shift in OCP and E_{corr} and, a significant decrease in i_{corr} . However, a reversal in trend is observed for other treated samples. The Nyquist, Bode impedance and Bode phase angle plots, of untreated and treated samples are shown in Fig. 8a, b and c, respectively. The Nyquist plots of untreated AISI 409 SS and those SMATed using 2 and 5 mm balls for 15 min are characterized by a single semicircle while those treated using 2 mm balls for 30 and 45 min and 5 mm balls for 30 min exhibit two semicircles, suggesting the involvement of single and two time constants, respectively. A single semicircle followed by a Warburg diffusion tail is observed for the sample treated using 5 mm balls for 45 min. Samples treated using 8 mm balls for 30 min exhibit a semicircle followed by a loop in the low frequency region. Different equivalent electrical circuit models are used to analyze the EIS spectra. The fittings obtained for the EIS data along with the corresponding equivalent electrical circuit model are shown in Fig. 9. In these models, R_s represents the solution resistance, R_f and R_{ct} are the film and charge transfer resistances whereas CPE₁ and CPE/CPE₂ are their respective constant phase elements. W is the Warburg diffusion element. L represents the inductance and R_L is the inductive resistance. The validity of these models is confirmed based on the better non-linear least square fitting of the experimental data within 5% error. The deviation in fitting observed for samples SMATed using 8 mm balls for 30 min is due to the pronounced dissolution through the defects created during the treatment. The EIS parameters of untreated and treated samples are compiled in Table 3. Compared to the untreated one, samples SMATed using 8 mm balls at all treatment time studied and those treated using 5 mm balls for 30 and 45 min exhibit a decrease in resistance and an increase in capacitance whereas a reversal in trend is observed for other treated samples. Current–time transients recorded at an impressed potential of $-100 \text{ mV}_{(\text{SCE})}$ for untreated and treated (2, 5 and 8 mm balls for 15 min) samples are shown in Fig. 10. The extent of increase in current is higher for the sample treated using 8 mm balls. The surface morphology of the SMATed (2, 5 and 8 mm balls for 15 min) AISI 409 SS samples after polarizing them from -250 to $+250 \text{ mV}_{(\text{SCE})}$ from their respective OCPs in 0.6 M NaCl, are shown in Fig. 11. The extent of corrosive attack is relatively less for samples treated using 2 and 5 mm balls whereas those treated using 8 mm balls exhibit severe corrosive attack. The corrosion behaviour of untreated and treated samples observed by OCP–time, polarization, EIS and CTT studies corroborate with each other. The surface morphology of the treated samples after polarization study support the inference made from electrochemical studies.

The corrosion behaviour of untreated and treated samples can be explained in terms of the surface roughness, passive film formation, extent of grain refinement, microstrain and defect density

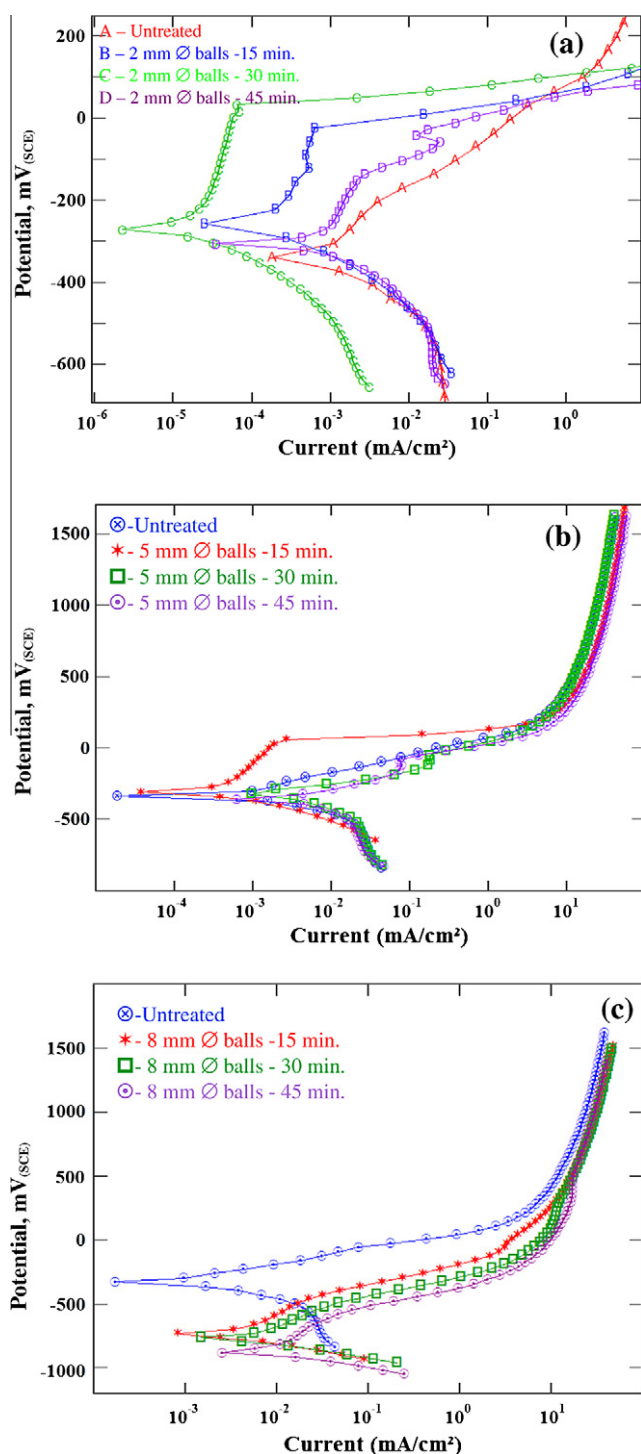


Fig. 7. Potentiodynamic polarization curves of AISI 409 SS in 0.6 M NaCl – untreated and after SMAT using (a) 2, (b) 5 and (c) 8 mm \varnothing balls for various duration of time.

Table 2

Corrosion potential (E_{corr}) and corrosion current density (i_{corr}) of untreated AISI 409 SS and samples SMATed using 2, 5 and 8 mm \varnothing 316L SS balls for 15, 30 and 45 min.

Treatment condition of AISI 409 SS	E_{corr} *, mV _(SCE)	i_{corr} * (μA/cm ²)
Untreated	-342	1.50
SMAT using 2 mm \varnothing 316L SS ball for 15 min	-259	0.28
SMAT using 2 mm \varnothing 316L SS ball for 30 min	-274	0.03
SMAT using 2 mm \varnothing 316L SS ball for 45 min	-305	0.84
SMAT using 5 mm \varnothing 316L SS ball for 15 min	-311	0.19
SMAT using 5 mm \varnothing 316L SS ball for 30 min	-322	2.18
SMAT using 5 mm \varnothing 316L SS ball for 45 min	-363	2.27
SMAT using 8 mm \varnothing 316L SS ball for 15 min	-730	3.05
SMAT using 8 mm \varnothing 316L SS ball for 30 min	-794	4.75
SMAT using 8 mm \varnothing 316L SS ball for 45 min	-882	6.50

* Average of three determinations.

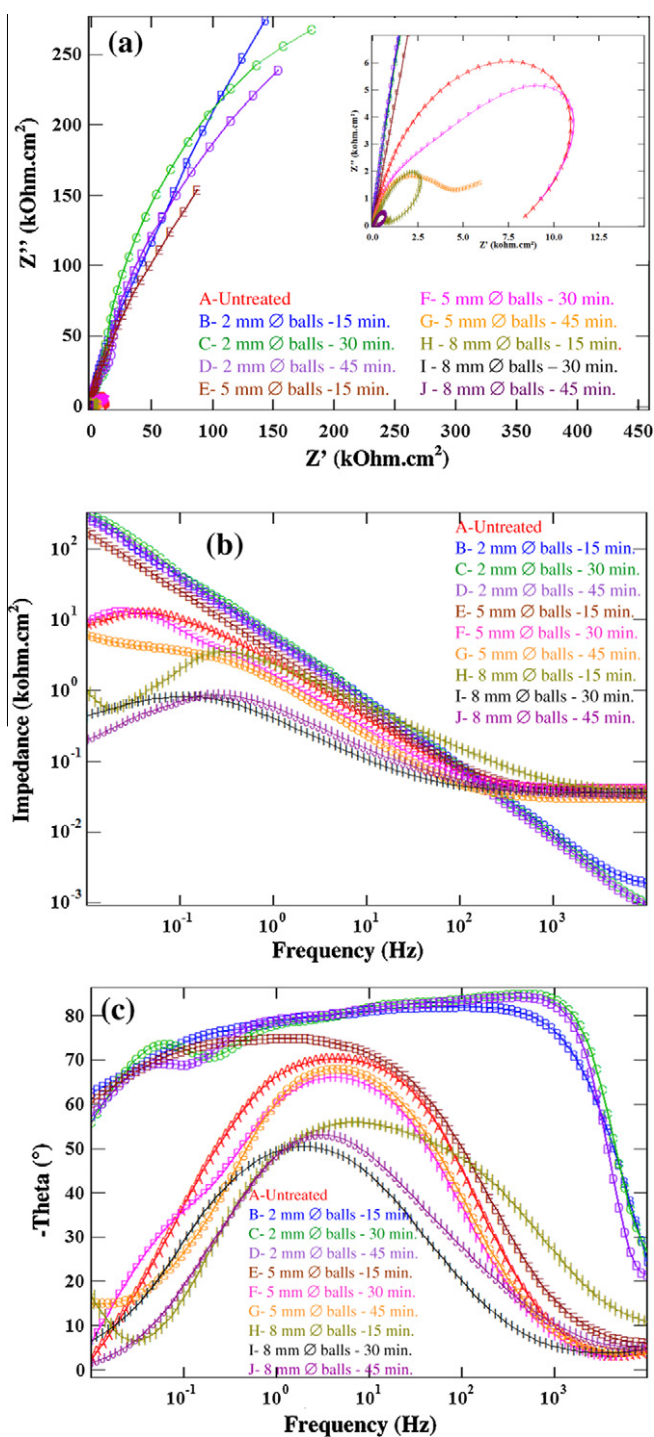


Fig. 8. The Nyquist (a), Bode impedance (b) and Bode phase angle (c) plots, of untreated AISI 409 SS and samples SMATed using 2, 5 and 8 mm \varnothing balls for 15, 30 and 45 min in 0.6 M NaCl recorded at their respective open circuit potentials.

induced during treatment. Surface roughness has a greater influence on the corrosion resistance [32–36]. In general, a smoother surface offers a better corrosion resistance and vice versa. In the present study, as explained in Section 3.1, SMAT has caused an increase in surface roughness and the extent of roughness is increased with ball size and treatment time (Table 1). Increase in roughness would lead to a decrease in electron work function (EWF) and increase the corrosion rate [32,33]. Increase in surface roughness has been shown to increase the metastable pits on AISI

301 grade stainless steel [33]. In addition, increase in roughness following thermal oxidation of CP-Ti and plasma electrolytic oxidation of AZ 91 Mg alloy has resulted in a decrease in corrosion rate [35,36]. It is also observed in the present study that increase in surface roughness by SMAT using 5 mm balls for 30 and 45 min and by 8 mm balls at all treatment time studied leads to a higher corrosion rate. In spite of the increase in roughness, samples treated using 2 mm balls at all treatment times studied and those treated using 5 mm balls for 15 min offer better corrosion resistance. Polarization studies reveal the formation of a passive film for these samples (Figs. 7a and b). This observation is further substantiated by the capacitive behaviour in the Nyquist plot (Fig. 8a) and by the higher impedance and higher phase angle maximum covering a large range of frequencies in the Bode impedance and phase angle plots (Fig. 8b and c). The formation of passive film at the above said treatment conditions could be attributed due to surface nanocrystallization. The possibility of improved passivity due to high temperature oxidation can be ruled out since the SMAT was performed under vacuum for the entire duration and the temperature of the sample is less than 100 °C. Lu et al. [6] have also reported that the temperature of the steel sample during SMAT lies in the range of 50–100 °C. In addition, XRD patterns of the all treated samples did not reveal the formation of any oxides. Hence, the improved surface passivity observed for SMATed samples could be due to the surface nanocrystallization rather than high temperature oxidation.

Grain refinement is an important factor in determining the corrosion resistance. In the present study, the multidirectional impact of the balls has caused a reduction in grain size at all treatment conditions. However, the corrosion rate is increased at certain conditions only. Grain refinement has been shown to increase the corrosion rate of stainless steel [11–13]. A decrease in grain size has also offered an improvement in corrosion resistance of γ -stainless steel [37] and increased the high temperature corrosion resistance of zirconium [38]. The higher corrosion resistance exhibited by commercially pure Ti after two passes of ECAP instead of eight passes (at which the smallest grain size is obtained) [39] and, a similar corrosion rate exhibited by pure Mg both in as-SMATed and after post annealing treatment [39] further substantiate this phenomenon. Irrespective of a similar grain size after treatment, a higher corrosion rate is observed for AZ31 magnesium alloy subjected to ECAE than conventional extrusion [19]. Hence, the corrosion behaviour of SMATed samples cannot be analyzed only in terms of grain size and other parameters such as defect density and microstrain should be considered.

The extent of deformation, defect density, microstrain and surface free energy has been correlated to the corrosion resistance of materials subjected to deformation by different methods [14,15,19,40]. According to Hamdy et al. [14] a 23% cold deformation of niobium containing stainless steel has resulted in an improvement in corrosion resistance in 3.5% NaCl whereas a subsequent increase in the extent of deformation to 40% and 50% lead to a decrease in corrosion resistance. Similarly, cold working of nitrogen-bearing 316L grade stainless steel up to 20% has been shown to enhance its pitting corrosion resistance whereas further increase in the extent of cold working to 30% and 40% has decreased the pitting resistance [15]. It has been demonstrated that dislocations created during deformation decreases the electron work function and reduces the energy barrier for electrochemical reactions [33,41–43]. Increase in dislocation density following deformation would provide a large number of active sites and promote the rate of corrosion [33,43,44]. The increase in density of dislocation has been attributed to the increase in corrosion rate of ECAE processed AZ31 magnesium alloy compared to samples subjected to conventional extrusion [19]. SMAT is believed to induce an extremely high free energy state in the near-surface region of the material being processed and based on their results Op't Hoog et al. [40] have

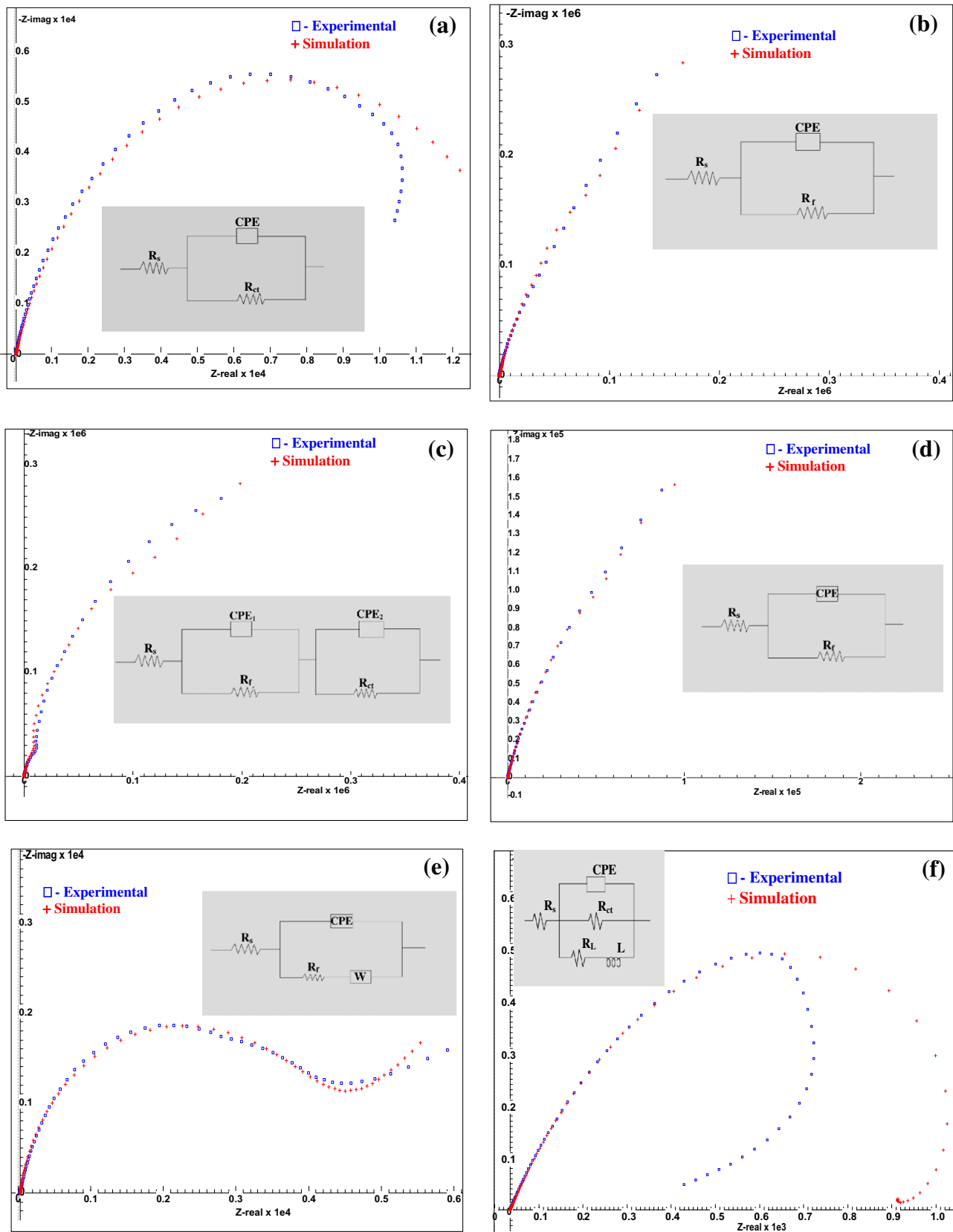


Fig. 9. Non-linear least square fitting obtained for the EIS data of untreated and SMATed AISI 409 SS: (a) untreated; (b) SMATed using 2 mm \varnothing balls for 15 min; (c) SMATed using 2 mm \varnothing balls for 45 min; (d) SMATed using 5 mm \varnothing balls for 15 min; (e) SMATed using 5 mm \varnothing balls for 45 min; and (f) SMATed using 8 mm \varnothing balls for 30 min.

confirmed that this results in an increase in corrosion rate of pure Mg despite a decrease in grain size. A similar phenomenon is also

expected for SMATed AISI 409 SS. Hence, the decrease in corrosion resistance of samples SMATed using 8 mm balls at all treatment

Table 3

EIS parameters of untreated AISI 409 SS and samples SMATed using 2, 5 and 8 mm \varnothing 316L SS balls for 15, 30 and 45 min in 0.6 M NaCl.

Treatment condition of AISI 409 SS	R_f (Ohm/cm ²)	CPE_1 (mho/s ⁿ /cm ²)	n	R_{ct} (Ohm/cm ²)	CPE/CPE_2 (mho/s ⁿ /cm ²)	n	W (mho s ^{0.5} /cm ²)	R_L (Ohm/cm ²)	L (Henri)
Untreated	–	–	–	1.30×10^4	9.80×10^{-5}	0.82	–	–	–
SMAT using 2 mm \varnothing balls for 15 min	9.53×10^5	2.80×10^{-5}	0.85	–	–	–	–	–	–
SMAT using 2 mm \varnothing balls for 30 min	5.90×10^5	4.20×10^{-5}	1.00	9.78×10^3	6.00×10^{-5}	0.95	–	–	–
SMAT using 2 mm \varnothing balls for 45 min	6.01×10^5	4.23×10^{-5}	0.95	9.82×10^3	5.60×10^{-5}	1.00	–	–	–
SMAT using 5 mm \varnothing balls for 15 min	5.21×10^5	5.16×10^{-5}	0.85	–	–	–	–	–	–
SMAT using 5 mm \varnothing balls for 30 min	9.05×10^3	7.28×10^{-4}	1.00	5.52×10^3	1.27×10^{-4}	0.82	–	–	–
SMAT using 5 mm \varnothing balls for 45 min	4.20×10^3	1.12×10^{-4}	0.85	–	–	–	2.3×10^{-3}	–	–
SMAT using 8 mm \varnothing balls for 15 min	–	–	–	9.90×10^3	1.00×10^{-4}	0.69	–	6.5×10^3	5.3×10^3
SMAT using 8 mm \varnothing balls for 30 min	–	–	–	2.10×10^3	9.90×10^{-4}	0.70	–	1.73×10^3	4.9×10^3
SMAT using 8 mm \varnothing balls for 45 min	–	–	–	2.40×10^3	8.59×10^{-4}	0.65	–	1.32×10^3	2.3×10^3

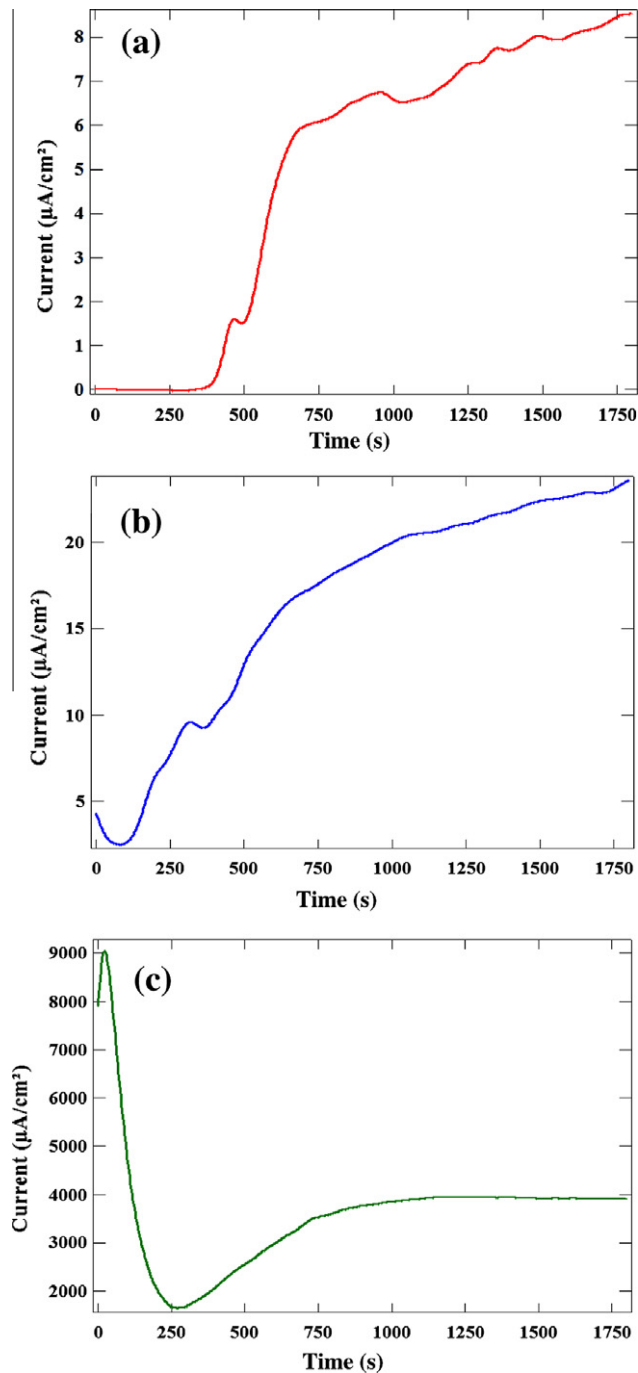


Fig. 10. Current–time transients of SMATed AISI 409 SS in 0.6 M NaCl at $-100 \text{ mV}_{(SCE)}$: (a) SMATed using 2 mm \varnothing balls for 15 min; (b) SMATed using 5 mm \varnothing balls for 15 min; and (c) SMATed using 8 mm \varnothing balls for 15 min.

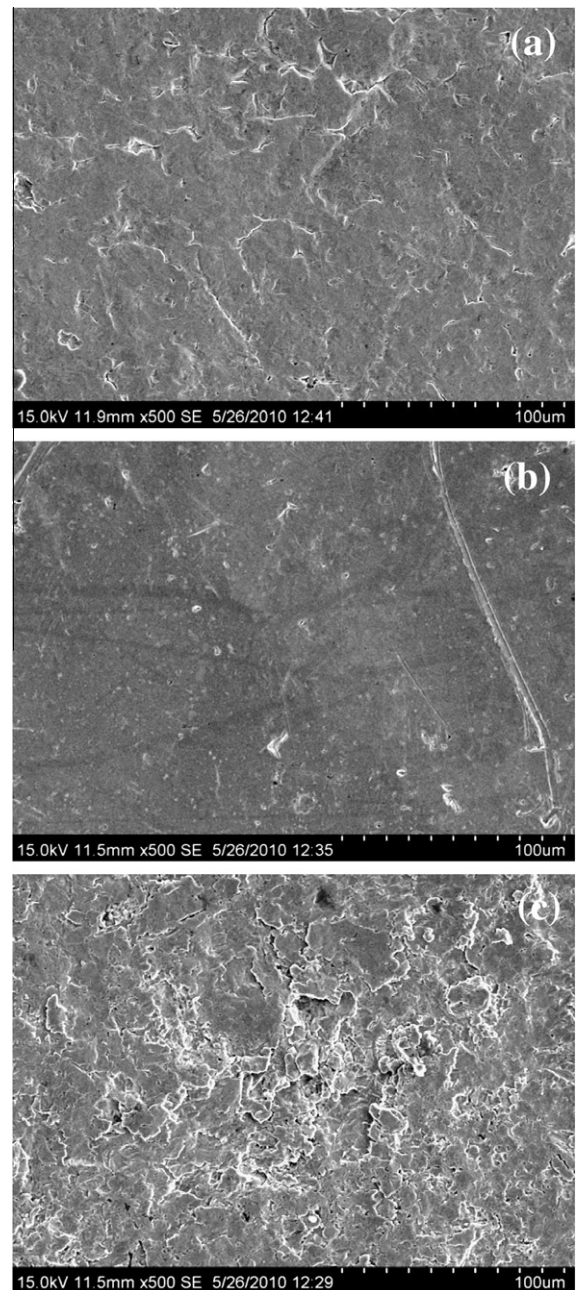


Fig. 11. Surface morphology of SMATed AISI 409 SS samples after polarizing them from -250 to $+250 \text{ mV}_{(SCE)}$ from their respective OCPs in 0.6 M NaCl: (a) SMATed using 2 mm \varnothing balls for 15 min; (b) SMATed using 5 mm \varnothing balls for 15 min; and (c) SMATed using 8 mm balls for 15 min.

time studied and those treated using 5 mm balls for 30 and 45 min is attributed to the increase in surface roughness, microstrain and defect density. The severe corrosion damage and delamination of the deformed region of samples treated using 8 mm balls for 15 min confirms penetration of the electrolyte through the defects created during SMAT (Fig. 11). The improvement in corrosion resistance observed for samples SMATed using 2 mm balls for 15, 30 and 45 min and 5 mm balls for 15 min is due to the surface nanocrystallization following SMAT, which promotes the formation of a passive film on the surface.

4. Conclusions

SMAT induces plastic deformation of AISI 409 SS with a high strain rate during each impact. SMAT enables the formation of a graded layer structure with nano-sized grains at the surface and sub-micron/micron sized grains at the intermediate region whereas the grains at the bulk remain largely unaffected. SMAT increased the surface roughness; increase in ball size and treatment time increased the roughness. The surface nanocrystallization induced by SMAT causes a small change in lattice parameter. The crystalline imperfections induced by the smaller grain size and the microstrain have resulted in broadening of the XRD peaks. Increase in treatment time leads to a decrease in grain size and increase in microstrain. The electrochemical studies reveal that SMAT using 8 mm balls for all treatment time studied and by 5 mm balls for 30 and 45 min decreases the corrosion resistance following the increase in microstrain and defect density induced during the treatment. In contrast, SMAT using 2 mm balls for 15, 30 and 45 min and by 5 mm balls for 15 min enables surface nanocrystallization, which promotes passive film formation and increases the corrosion resistance. The study concludes that the corrosion resistance of SMATed AISI 409 SS in 0.6 M NaCl depends on surface nanocrystallization, extent of grain refinement and decrease in grain size and, increase in microstrain and defect density, induced during treatment.

Acknowledgement

The authors express their sincere thanks to the Director, National Metallurgical Laboratory, Jamshedpur, for his constant support and encouragement to carry out this research work and permission to publish this paper.

References

- [1] C.C. Koch, I.A. Ovid'ko, S. Seal, S. Veprek, *Structural Nanocrystalline Materials: Fundamentals and Applications*, Cambridge University Press, Cambridge, 2007.
- [2] H. Gleiter, *Prog. Mater. Sci.* 33 (1989) 223–315.
- [3] K. Lu, *Mater. Sci. Eng., R* 16 (1996) 161–221.
- [4] C.C. Koch, *Rev. Adv. Mater. Sci.* 5 (2003) 91–99.
- [5] K. Lu, J. Lu, *J. Mater. Sci. Technol.* 15 (1999) 193–197.
- [6] K. Lu, J. Lu, *Mater. Sci. Eng., A* 375–377 (2004) 38–45.
- [7] R. Mishra, R. Balasubramaniam, *Corros. Sci.* 46 (2004) 3019–3029.
- [8] L. Wang, Y. Lin, Z. Zeng, W. Liu, Q. Xue, L. Hu, J. Zhang, *Electrochim. Acta* 52 (2007) 4342–4350.
- [9] M.R. Zamanzad-Ghavidel, K. Raeissi, A. Saatchi, *Mater. Lett.* 63 (2009) 1807–1809.
- [10] Sh. Hassani, K. Raeissi, M. Azzi, D. Li, M.A. Golozar, J.A. Szpunar, *Corros. Sci.* 51 (2009) 2371–2379.
- [11] Y. Li, F. Fang, G. Liu, *Corrosion* 60 (2004) 891–896.
- [12] Y.W. Hao, B. Deng, C. Zhong, Y.M. Jiang, J. Li, *J. Iron Steel Res. Int.* 16 (2009) 68–72.
- [13] A.Q. Lu, Y. Zhang, Y. Li, G. Liu, Q.H. Zhang, C.M. Liu, *Acta Metall. Sinica* 19 (2006) 183–189.
- [14] A.S. Hamdy, E. El-Shenawy, T. El-Bitar, *Int. J. Electrochem. Sci.* 1 (2006) 171–180.
- [15] U. Kamachi Mudali, P. Shankar, S. Ningshen, R.K. Dayal, H.S. Khatak, Baldev Raj, *Corros. Sci.* 44 (2002) 2183–2198.
- [16] L. Peguet, B. Malki, B. Baroux, *Corros. Sci.* 49 (2007) 1933–1948.
- [17] H.S. Lee, D.S. Kim, J.S. Jung, Y.S. Pyoun, K. Shin, *Corros. Sci.* 51 (2009) 2826–2830.
- [18] B.N. Mordiyuk, G.I. Prokopenko, M.A. Vasylyev, M.O. Iefimov, *Mater. Sci. Eng., A* 458 (2007) 253–261.
- [19] G. Ben Hamu, D. Eliezer, L. Wagner, *J. Alloys Compd.* 468 (2009) 222–229.
- [20] D. Song, A. Ma, J. Jiang, P. Lin, D. Yang, J. Fan, *Corros. Sci.* 52 (2010) 481–490.
- [21] K. Elayaperumal, P.K. De, J. Balachandra, *Corrosion* 28 (1972) 269–273.
- [22] G. Salvago, G. Fumagalli, D. Sinigaglia, *Corros. Sci.* 23 (1983) 515–523.
- [23] D.A. Baranov, I.V. Leirikh, E.S. Myznikova, *Prot. Met.* 40 (2004) 254–256.
- [24] D.C. Silverman, "Tutorial on polexpertm and the cyclic potentiodynamic polarization technique," http://www.argentumsolutions.com/tutorials/polexpert_tutorialpg4.html.
- [25] Satendra Kumar, T.S.N. Sankara Narayanan, *J. Dent.* 36 (2008) 500–507.
- [26] Satendra Kumar, T.S.N. Sankara Narayanan, *J. Alloys Compd.* 479 (2009) 699–703.
- [27] Satendra Kumar, T.S.N. Sankara Narayanan, S. Ganesh Sundara Raman, S.K. Seshadri, *Mater. Chem. Phys.* 119 (2010) 337–346.
- [28] Satendra Kumar, T.S.N. Sankara Narayanan, S. Ganesh Sundara Raman, S.K. Seshadri, *Corros. Sci.* 52 (2010) 711–721.
- [29] Satendra Kumar, T.S.N. Sankara Narayanan, S. Saravana Kumar, Influence of fluoride ion on the electrochemical behaviour of β -Ti alloy for dental implant application, *Corros. Sci.* 52 (2010) 1721–1727.
- [30] F.M. Bayoumi, W.A. Ghanem, B.G. Ateya, *Int. J. Electrochem. Sci.* 1 (2006) 258–267.
- [31] ACM Instruments Instruction Manual, <http://www.acminstruments.com/media/pdf/v4manual.pdf> p. 15.
- [32] S. Yin, D.Y. Li, R. Bouchard, *Wear* 263 (2007) 801–807.
- [33] S. Yin, D.Y. Li, R. Bouchard, *Metall. Mater. Trans. A* 38A (2007) 1032–1040.
- [34] T. Hong, M. Nagumo, *Corros. Sci.* 39 (1997) 1665–1672.
- [35] E. Arslan, Y. Totik, E. Demirci, A. Alsaran, *J. Mater. Eng. Perform.* 19 (2010) 428–433.
- [36] D.Y. Hwang, B.Y. Yoo, J.Y. Cho, D.H. Lee, D.H. Shin, *Electrochim. Acta* 54 (2009) 5479–5485.
- [37] A. Di Schino, J.M. Kenny, *J. Mater. Sci. Lett.* 21 (2002) 1631–1634.
- [38] X.Y. Zhang, M.H. Shi, C. Li, N.F. Liu, Y.M. Wei, *Mater. Sci. Eng., A* 448 (2007) 259–263.
- [39] M. Hoesinia, A. Shahryari, S. Omanovic, J.A. Szpunar, *Corros. Sci.* 51 (2009) 3064–3067.
- [40] C. Op't Hoog, N. Birbilis, Y. Estrin, *Adv. Eng. Mater.* 10 (2008) 579–582.
- [41] D.Y. Li, *Phys. Status Solidi, A* 191 (2002) 427–434.
- [42] W. Li, D.Y. Li, *Mater. Sci. Technol.* 18 (2002) 1057–1062.
- [43] W. Li, D.Y. Li, *Appl. Surf. Sci.* 240 (2005) 388–392.
- [44] Songbo Yin, D.Y. Li, *Mater. Sci. Eng., A* 394 (2005) 266–276.